Interfacial spin glass state and exchange bias in manganite bilayers with competing magnetic orders

Tendeloo, G. Van; Ding, J. F.; Lebedev, O. I.; Turner, S.; Tian, Y. F.; Hu, W. J.; Seo, J. W.; Panagopoulos, C.; Prellier, W.; Wu, T.

2013

Ding, J. F., Lebedev, O. I., Turner, S., Tian, Y. F., Hu, W. J., Seo, J. W., et al. (2013). Interfacial spin glass state and exchange bias in manganite bilayers with competing magnetic orders. Physical Review B - Condensed Matter and Materials Physics, 87(5), 054428-.

https://hdl.handle.net/10356/80082

https://doi.org/10.1103/PhysRevB.87.054428

Interfacial spin glass state and exchange bias in manganite bilayers with competing magnetic orders

J. F. Ding,[1] O. I. Lebedev,[2] S. Turner,[3] Y. F. Tian,[1] W. J. Hu,[1] J. W. Seo,[1,*] C. Panagopoulos,[1] W. Prellier,[2] G. Van Tendeloo,[3] and T. Wu[1,†]

[1]*Division of Physics and Applied Physics, School of Physical and Mathematical Sciences, Nanyang Technological University, Singapore 637371, Singapore*

[2]*Laboratoire CRISMAT, UMR 6508, CNRS ENSICAEN, F-14050 Caen, France*

[3]*EMAT, University of Antwerp, Groenenborgerlaan 171, B-2020 Antwerpen, Belgium*

(Received 1 September 2012; published 21 February 2013)

The magnetic properties of manganite bilayers composed of G-type antiferromagnetic (AFM) $SrMnO_3$ and double-exchange ferromagnetic (FM) $La_{0.7}Sr_{0.3}MnO_3$ are studied. A spin-glass state is observed as a result of competing magnetic orders and spin frustration at the $La_{0.7}Sr_{0.3}MnO_3/SrMnO_3$ interface. The dependence of the irreversible temperature on the cooling magnetic field follows the Almeida-Thouless line. Although an ideal G-type AFM $SrMnO_3$ is featured with a compensated spin configuration, the bilayers exhibit exchange bias below the spin glass freezing temperature, which is much lower than the Néel temperature of SMO, indicating that the exchange bias is strongly correlated with the spin glass state. The results indicate that the spin frustration that originates from the competition between the AFM super-exchange and the FM double-exchange interactions can induce a strong magnetic anisotropy at the $La_{0.7}Sr_{0.3}MnO_3/SrMnO_3$ interface.

DOI: 10.1103/PhysRevB.87.054428 PACS number(s): 75.70.Cn, 71.27.+a

I. INTRODUCTION

Due to the coexisting spin, charge and orbital degrees of freedom and their reconstruction, interfaces between different oxides in artificially layered heterostructures are expected to exhibit much richer physics than their conventional semiconductor counterparts.[1–4] Recent advances in the fabrication of high-quality epitaxial interfaces between perovskite oxides have led to a rapid surge of interest in the study of new interfacial electronic states, and some fascinating phenomena have been revealed.[5–8] Heterostructures composed of magnetically active transition metal oxides are especially interesting because of the intricate spin-dependent exchange interaction at the interfaces.[9–17] For example, ferromagnetism has been observed at interfaces between two antiferromagnets or between an antiferromagnet and a paramagnet.[10,18–22] It is well recognized that epitaxial heterostructures of mixed-valence manganites offer excellent opportunities to exploit such emerging magnetic phenomena and shed light on the competing interactions at the interfaces.

One interfacial phenomenon that has captured lots of attention for several decades is the exchange bias (EB) in heterostructures of ferromagnetic (FM) and antiferromagnetic (AFM) materials. In magnetic hysteresis loop measurements, the EB effect manifests itself as a shift along the field axis, and the additional unidirectional anisotropy is attributed to the exchange interaction between the FM and AFM spins at the interface. Because of its importance in spintronic applications, a large amount of experimental and theoretical work has been undertaken to discern the nature of interfacial AFM/FM exchange coupling. Although several theoretical models have been proposed to explain the EB behavior,[23–31] they are challenged by emerging experimental results.

In particular, issues arise when the AFM layer possesses a G-type antiferromagnetic order. In most of the existing models, an uncompensated AFM interface is a prerequisite for the emergence of EB; therefore G-type AFM, where all the nearest-neighboring spins at the AFM/FM interface are compensated by each other, is not expected to pin the FM spins via an exchange coupling. Although some earlier reports considered some extrinsic factors, such as random defects[25] and interface roughness,[27] which may affect the exchange coupling, there remain open questions regarding the magnetic characteristics of the interface between G-type AFM and FM layers. Recently, EB was observed at epitaxial heterostructures involving G-type AFM layers such as $BiFeO_3$,[32–36] where Dzyaloshinskii-Moriya interaction and ferroelectric polarization were proposed to play important roles.[31] Perovskite-structured manganites are well suited to investigate this issue because they boast rich phase diagrams with a myriad of magnetic orders.[37–39] Furthermore, epitaxial heterostructures can be routinely achieved as a result of their structural compatibility.

In this paper, we studied the magnetic properties of bilayer heterostructures composed of G-type AFM $SrMnO_3$ (SMO) and FM $La_{0.7}Sr_{0.3}MnO_3$ (LSMO). Since both layers are manganites, a large exchange coupling can be expected at the LSMO/SMO interface due to the direct Mn-O-Mn exchange interaction. Indeed, EB effects have been demonstrated before in all-manganite heterostructures, in particular, in superlattices,[40–43] sandwich-type multilayers[44] and bilayers[45] of $La_{2/3}Ca_{1/3}MnO_3/La_{1/3}Ca_{2/3}MnO_3$. In this combination, the $La_{1/3}Ca_{2/3}MnO_3$ layer, which has a noncollinear AFM spin order with a Néel temperature T_N of about 170 K,[46] magnetically couples to the FM $La_{2/3}Ca_{1/3}MnO_3$ layer.

SMO and $LaMnO_3$ (LMO) are the two end members of the $La_{1-x}Sr_xMnO_3$ series. Considering that LMO has an A-type AFM order,[47] we also explored the magnetic properties of the LSMO/LMO bilayers. However, because the cation vacancies in LMO produce a weak magnetism in the bilayers,[47,48] we could not unambiguously determine the interfacial magnetic properties. Therefore we focus on the LSMO/SMO bilayers in this work.

In the simplified scheme of structural and spin orders illustrated in Fig. 1, the two nearest-neighboring spins in the

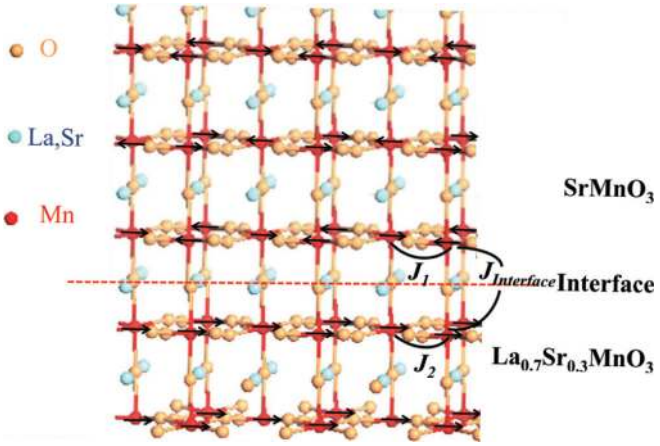

FIG. 1. (Color online) Idealized illustration of the lattice structure and the simplified spin configuration at the interface of LSMO/SMO bilayer. The arrows show the spin directions in the G-type AFM SMO and FM LSMO without considering the magnetic frustration at the interface. J_1, J_2, and $J_{\text{Interface}}$ represent the AFM superexchange interaction, the FM double-exchange interaction, and the interface exchange coupling, respectively.

FM LSMO layer at the interface will be subject to an opposite pinning force from the proximate AFM SMO layer. As a result, significant spin frustration at the interface is expected in the bilayers. Indeed, our systematic study of the magnetic properties of the LSMO/SMO bilayers suggests a notable spin-glass state, which is absent in the reference single layers. Furthermore, we observed the EB effect in the bilayers, and the development of such a unidirectional anisotropy appears to be closely correlated with the spin-glass state at the LSMO/SMO interface.

II. EXPERIMENTAL DETAILS

LSMO/SMO bilayers were grown on atomically flat TiO_2-terminated (100)-oriented $SrTiO_3$ (STO) substrates using pulsed laser deposition (PLD). The frequency of the excimer laser was 2 Hz and 10 Hz for the LSMO and SMO layers, respectively. The energy fluence of the laser was $\sim$1.5 J/cm^2. The growth took place at a substrate temperature of 750 °C and an oxygen pressure of 20 Pa. After growth, the samples were *in situ* annealed in an O_2 atmosphere of 1 bar for one hour before slowly cooling down to room temperature. As reference samples, SMO and LSMO single layers were grown on STO substrates under the same conditions. Magnetic properties of the samples were measured by a superconducting quantum interference device (SQUID, Quantum Design) magnetometer. The applied magnetic field is always parallel to the film plane and along the [010] direction of the STO substrate. For the field-cooled (FC) and zero-field-cooled (ZFC) magnetization measurements, the sample was cooled down from 400 K to the desired temperature with and without the magnetic field, respectively. Both the ZFC and FC magnetization versus temperature (M-T) curves were measured during the warming process. The hysteresis loops were measured after FC from 400 K under a 5000 Oe magnetic field. For the measurement of the relaxation of thermal remnant magnetization, the sample was field cooled under a magnetic field of 0.1 kOe from

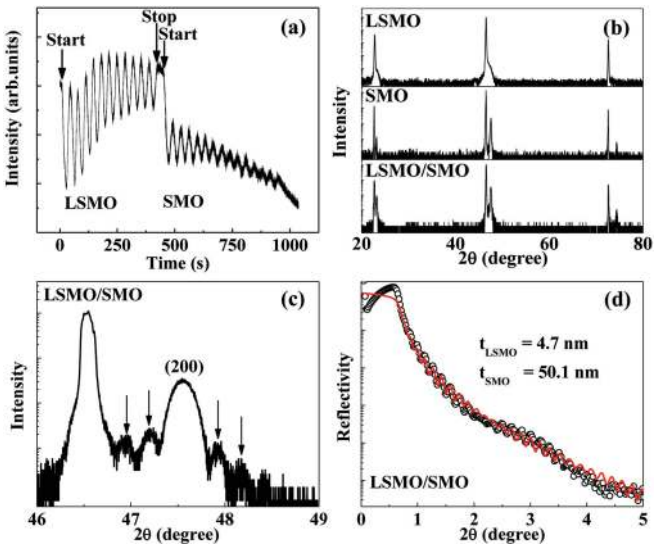

FIG. 2. (Color online) (a) RHEED oscillations during the growth of the LSMO/SMO bilayer. (b) XRD data for LSMO/SMO bilayer and the reference LSMO and SMO single layers grown on STO(100) substrates. (c) Enlarged view around the (200) diffraction peak of the bilayer. The arrows mark the positions of fringe peaks. (d) Reflectivity data of the LSMO/SMO bilayer. The hollow cycles are the experiment data, and the red line is the fitting to the data.

400 K to the predetermined temperatures, and then the time dependence of the magnetization was recorded immediately after the magnetic field decreased to zero.

The structural characterization was performed by x-ray diffraction (XRD) and (scanning) transmission electron microscopy [(S)TEM]. The XRD θ-2θ scan and reflectivity were studied with a high-resolution x-ray diffractometer (Smartlab, Rigaku, Japan). TEM and high-resolution TEM (HRTEM) studies were carried out using a FEI Tecnai G2 30 UT microscope operated at 300 kV. Aberration-corrected high-angle annular dark field scanning TEM (HAADF-STEM) experiments were performed on a Titan "cube" microscope, equipped with an aberration corrector for the probe-forming lens and operated at 300 kV. The convergence semi-angle alpha used for imaging was 21.5 mrad; the inner detection semi-angle beta of the HAADF detector was 50 mrad. Cross-section specimens were prepared by cutting the samples along the (100) STO plane, followed either by mechanical polishing and ion-beam milling in a JEOL Ion Slicer or by focussed ion-beam (FIB) slicing in an FEI Helios FIB-SEM.

III. RESULTS AND DISCUSSION

The reflection high-energy electron diffraction (RHEED) data in Fig. 2(a) suggest that the LSMO layer was grown on the STO substrate with a layer-by-layer mode and the oscillations become weaker as the SMO layer grew thicker. The nominal thicknesses of the LSMO layer and the SMO layer are 4.6 nm (12 unit cells) and 50 nm, respectively. The XRD θ-2θ scans for the LSMO/SMO bilayer and the reference single layers in Fig. 2(b) show good crystallinity and c-axis orientation. In the LSMO/SMO bilayer, the diffraction peaks of the LSMO layer overlap with those of the substrate and the SMO layer. Although the exact magnitude of strain is difficult

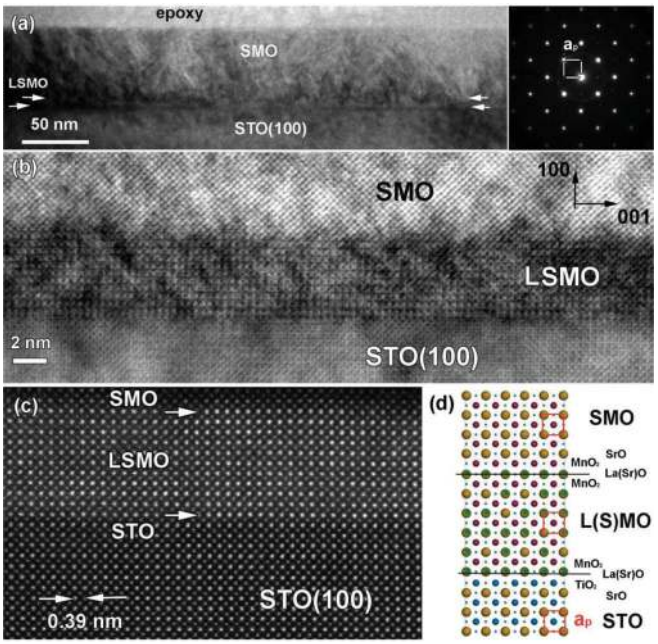

FIG. 3. (Color online) (a) Low-magnification cross-section bright-field TEM image and the corresponding ED pattern of the SMO/LSMO bilayer on STO(100), imaged along the $[100]_{STO}$ zone axis orientation. The LSMO layer (darker contrast) is indicated by white arrows. (b) HRTEM image of the SMO/LSMO/STO(100) structure observed along the $[100]_{STO}$ zone axis. (c) High-resolution HAADF-STEM image of the bilayer. The STO substrate, LSMO and SMO layers can be clearly distinguished because of the difference in average Z number. (d) Idealized structural model of the LSMO/SMO bilayer on the STO substrate (the yellow, blue, smaller light blue, green, and red spheres represent Sr, Ti, O, La, and Mn atoms, respectively).

to determine, the LSMO layer should be under a tensile strain due to its coherent growth on the STO substrate. The c-axis lattice constant of the SMO layer is 3.826 Å, which is smaller than the bulk value of 3.857 Å, indicating that the SMO layer is also under a tensile strain. No impurity phase was observed for any of the samples. As shown in Fig. 2(c), Laue fringes were observed around the (200) diffraction peak, which suggests a flat surface of the sample. The reflectivity data are shown in Fig. 2(d), and through fitting the thicknesses of LSMO and SMO layer are estimated to be $t_{LSMO} = 4.7 \pm 0.1$ nm and $t_{SMO} = 50.1 \pm 0.4$ nm, respectively.

The low-magnification cross-section TEM image of the SMO/LSMO/STO(100) bilayer film in Fig. 3(a) confirms the layer thicknesses. No secondary phase or amorphous layer was observed. The corresponding electron diffraction (ED) over an area covering the substrate and the bilayer film can be unraveled as the superposition of patterns produced by the STO substrate, LSMO and SMO. Despite the difference in lattice parameters and crystal structure of bulk LSMO ($a = 5.457$, $R\text{-}3c$), SMO ($a = 5.443$, $c = 9.07$, $P63/mmc$) and STO ($a = 3.905$, $Pnma$), the ED pattern shows a single cubic-zone diffraction pattern. No splitting or elongations of the diffraction spots were observed, indicating a perfect heteroepitaxial growth of the bilayer. It can be seen from the HRTEM image in Fig. 3(b) that the film is coherently grown on the STO substrate. No misfit dislocations were observed along the interfaces, confirming that the bilayer is fully strained.

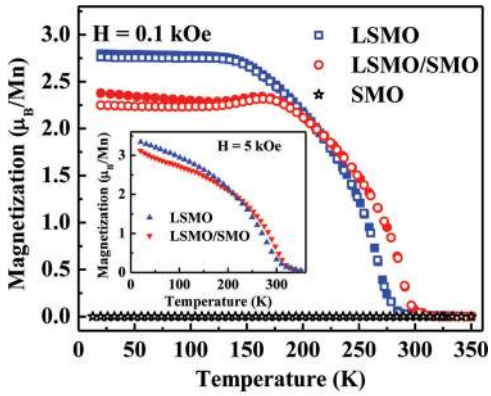

FIG. 4. (Color online) Temperature dependence of the magnetization measured on the LSMO/SMO bilayer as well as the LSMO and the SMO reference single layers under a magnetic field of 0.1 kOe. The solid and the empty symbols are the FC and ZFC data, respectively. The inset shows the M-T curves of the samples measured under a magnetic field of 5 kOe.

The high-resolution HAADF-STEM (Z-contrast) image in Fig. 3(c) provides direct evidence of the sharp interface between the layers. As the contrast in this technique is related to the atomic number Z, the STO substrate and the SMO layer appear darker than the LSMO layer because of their lower average Z numbers (Sr-38, Ti-22, Mn-25, and La-57). As expected, we observed steps and terrace structures at the interfaces due to the small miscut angle of the STO substrate. Figure 3(d) shows the schematic stacking sequence and the interface structure based on the experimental Z-contrast image. Since the STO substrate is TiO_2 terminated, the interface between the STO substrate and the first LSMO layer can be represented as -TiO_2-SrO-TiO_2-La(Sr)O-MnO_2-, and the LSMO/SMO interface as -La(Sr)O-MnO_2-SrO-MnO_2-.

The magnetization versus temperature (M-T) data measured under 0.1 kOe for the bilayer LSMO/SMO and the single layer LSMO and SMO reference films are shown in Fig. 4. The ferromagnetic transition temperature T_c determined by the differential of the M-T curves are 288 and 271 K for the bilayer and the LSMO single layer, respectively. The origin of the slightly higher T_c observed in the bilayer is not clear at the moment. The magnetic signal of the reference SMO layer is weak because of its AFM nature. To determine the Néel temperature T_N, we grew a thick SMO film of 300 nm and the measured temperature dependence of magnetization suggests a T_N of 227 K, which is close to the reported bulk value of ~240 K.[49] Nevertheless, the fact that the contribution of the SMO layer to the overall magnetic signal is negligible facilitates the interpretation of magnetization data.

There are two prominent features in the bilayer data in Fig. 4: a peak in both ZFC and FC M-T curves, and a bifurcation between the two curves below the irreversibility temperature T_{irr}. These features have been reported for several commonly known magnetic systems such as spin glass,[50,51] cluster glass,[52–54] and superparamagnet.[51,55] But the characteristics of the curves have subtle differences from superparamagnets, which often exhibit monotonously increasing FC

magnetization on decreasing temperature.[51] We can also exclude cluster glass systems because their peak temperature in the *M-T* curves is usually lower than T_{irr}, whereas in our case the two temperatures are very close to each other.[53] Thus the temperature dependence of the magnetization in Fig. 4 most likely suggests a spin glass state in the LSMO/SMO bilayer. On the other hand, for the LSMO single layer with the same thickness of 4.7 nm, the ZFC magnetization data overlap well with the FC one, which suggests that the spin glass state in the LSMO/SMO bilayer cannot be attributed to the "bulk" parts of the films, instead it must be related to the magnetic coupling at the LSMO/SMO interface. Moreover, the weaker magnetization of the bilayer compared with that of the LSMO single layer at low temperatures suggests that the spin glass state occurs at least partially in the LSMO layer and disturbs the FM spin order; otherwise, the overall magnetization would stay roughly the same since the SMO layer contributes very little to the overall magnetization.

We also measured the *M-T* curves of the samples under a larger field of 5 kOe as shown in the inset of Fig. 4. For ideal ferromagnetic $La_{1-x}Sr_xMnO_3$ with all the spins parallel to each other, the low-temperature saturation moment as expected from the 3*d* electrons present in manganese ions should be[56]

$$\begin{aligned} M_S &= x\mathrm{Mn}^{3+}(S=4/2)+(1-x)\mathrm{Mn}^{4+}(S=3/2) \\ &= 4x\mu_B + 3(1-x)\mu_B. \end{aligned} \tag{1}$$

For $x = 0.3$, M_S should be $3.3\mu_B$, which agrees well with the LSMO data shown in the inset of Fig. 4. Under a magnetic field of 5 kOe, the magnetization of the LSMO/SMO bilayer approaches that of the single LSMO layer, suggesting that the magnetic frustration is suppressed to a certain degree by the strong magnetic field, but at low temperatures, the magnetization of the LSMO/SMO bilayer remains lower than that of the reference LSMO layer.

Figure 5(a) shows the *M-T* curves for the LSMO/SMO bilayer measured under different magnetic fields, and it can clearly be observed that the irreversibility temperature decreases with the increasing field. As shown in Fig. 5(b), the field dependence of the T_{irr} follows the Almeida-Thouless (AT) line:[57]

$$H(T_{irr})/\Delta J \propto (1 - T_{irr}/T_F)^{3/2}, \tag{2}$$

where T_F is the zero-field spin-glass freezing temperature and ΔJ is the width of the distribution of the exchange interaction. Although the critical line is predicted for ideal Ising spin systems, the collapse of the experimental data to the AT line in Fig. 5(b) supports the existence of spin-glass behavior in LSMO/SMO bilayer.[50,58,59] The fitting gives a freezing temperature $T_F = 178$ K. To further demonstrate the spin-glass behavior in the LSMO/SMO bilayer, we studied the magnetic relaxation and the data are show in Fig. 5(c). The relaxation of the thermal remanent magnetization was measured at three temperatures: 100 K where the spins are frozen, 160 K, which is just below the spin-glass freezing temperature T_F, and 230 K, which is above T_F. The decay curves can be fitted by a stretched-exponential function:

$$M(t) = M_0 \exp[-C(\omega t)^{1-n}/(1-n)], \tag{3}$$

where C is the exponential factor and ω is the relaxation frequency.[60] The fitting parameter n was determined to be 0.8727 at 160 K and 0.6977 at 100 K, which are similar to the values reported for other spin glass systems such as AgMn, i.e., $n \sim 0.87$ at T_F and ~0.67 in the temperature region far below T_F.[60] For the temperature 230 K, the thermal remnant magnetization is quite small, and no clear relaxation was observed. These data clearly suggest that the magnetic relaxation and glassy behavior are most prominent near the spin freezing temperature T_F. We also tried to study the spin-glass state in the bilayer using ac susceptibility;[53,59,61] however, the signal of the thin film was too weak to achieve reliable measurements.

In the LSMO/SMO bilayer, the spin glass state as a result of magnetic frustration can be linked to the competition between the AFM super-exchange and the FM double-exchange interactions at the interface. In fact, such a competition has been reported in previous studies on manganite superlattices.[21,22,62,63] As illustrated in Fig. 1, at the interface of G-type AFM and FM layers, the nearest neighboring FM spins will always be influenced by an opposite pinning force from the AFM layer regardless whether the interface exchange coupling is FM or AFM type. As a result, the FM spin shows a frustrated behavior when the interface coupling is strong enough. The spin frustration could appear in both the AFM and FM layers, and the characteristics of the frustrated regions are determined

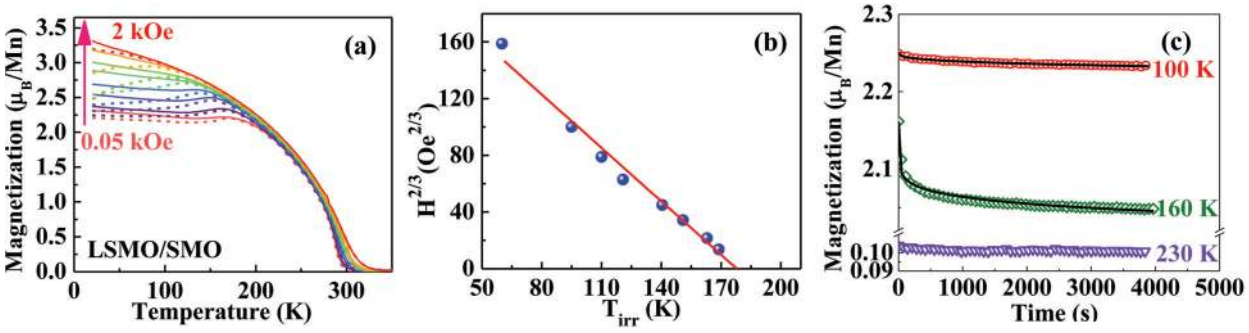

FIG. 5. (Color online) (a) *M-T* curves of the LSMO/SMO bilayer measured under different magnetic fields ($H = 0.05$, 0.1, 0.2, 0.3, 0.5, 0.7, 1, and 2 kOe). The solid and dashed lines are the ZFC and the FC data, respectively. (b) Corresponding plot of $H^{2/3}$ vs T_{irr}. The red line is the fitting to Eq. (2). (c) Time dependence of the thermal remnant magnetization after field cooling under a magnetic field of 0.1 kOe from 400 K to various temperatures. The lines are the fittings to Eq. (3).

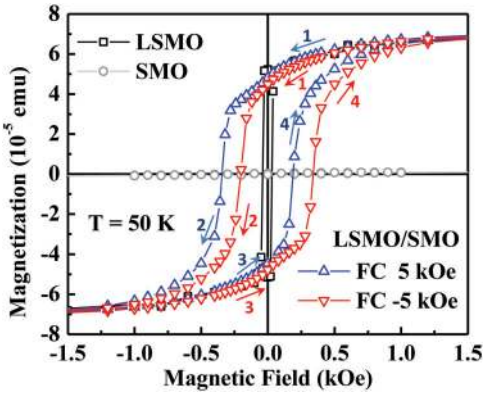

FIG. 6. (Color online) *M-H* loops measured on the LSMO/SMO bilayer and the reference single layers at 50 K after field cooled from 400 K. The measurement range is between -5 and 5 kOe. For clarity, only the data between -1.5 and 1.5 kOe are shown. The arrows and numbers show the scanning sequence of the magnetic field.

by the stability of AFM and FM exchange interactions and the coupling strength between the layers.

Figure 6 shows the hysteresis loops of the LSMO/SMO bilayer and the reference single layers measured at 50 K after field cooling from 400 K. An obvious shift of the hysteresis loop, a signature of the exchange bias, was observed in the LSMO/SMO bilayer. The EB field $H_{EB} = |H_+ + H_-|/2$ is 80 Oe at 50 K, where H_+ and H_- denote the right and left coercivity fields, respectively. Meanwhile, the coercivity defined as $H_C = |H_+ - H_-|/2$ significantly increases from 30 Oe for the LSMO single layer to 230 Oe for the bilayer. For the SMO single layer, the magnetization is negligible. Moreover, we did not observe any EB in the LSMO single layer, thus the EB in LSMO/SMO bilayer unambiguously originates from the interface coupling. We note here that the G-type AFM order in the SMO layer is not expected to pin the FM spins of the LSMO layer since the nearest-neighboring spins are compensated by each other. However, the spin order of the SMO at the interface could be modified and different from that of the ideal bulk form. It was reported that in $LaMnO_3/SrMnO_3$ superlattices with thin layer thicknesses (up to four unit cells),[64] the entire superlattices exhibit A-type AFM order, i.e., the spins of the SMO layer does not possess a G-type order any more. In our LSMO/SMO bilayers, the strong magnetic coupling and frustration may modify the interfacial spin orders, and the detailed spin configuration at the interface clearly warrants future investigation.

The hysteresis loops in Fig. 7(a) measured at different temperatures for the LSMO/SMO bilayer show that both H_{EB} and H_C increase with decreasing temperature. The temperature-dependent trend is illustrated in Fig. 7(b), and the Néel temperature T_N of bulk SMO and the spin-glass freezing temperature T_F of LSMO/SMO bilayer are also marked. One can see that the EB appears below a blocking temperature T_B of about 130 K, which is much lower than T_N. Therefore it is clear that above T_B the AFM order in the SMO layer is not stable enough to provide the unidirectional anisotropy, which depends on the ratio of the average interfacial coupling energy to the domain wall energy.[65] On the other hand, T_B is quite close to the freezing temperature T_F of the interfacial spin glass

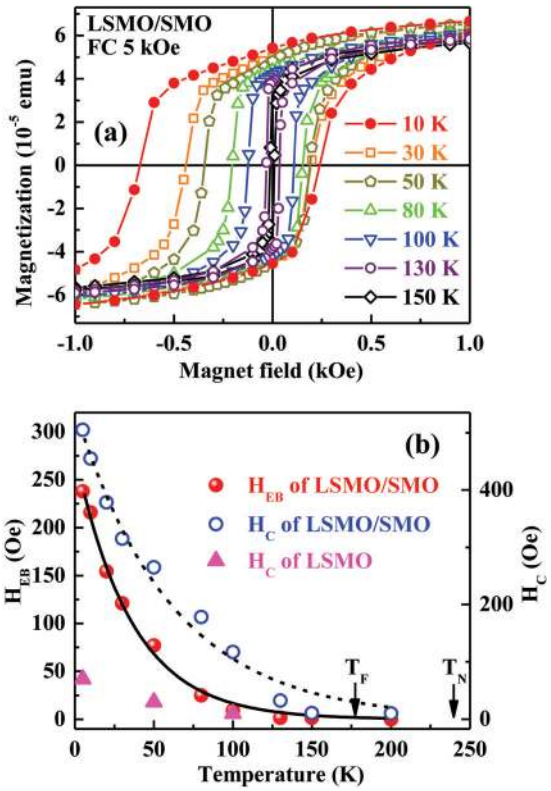

FIG. 7. (Color online) (a) *M-H* loops for the LSMO/SMO bilayer measured at different temperatures. For clarity, only the data between -1 and 1 kOe are shown in the figures, while the actual measurements took place between -5 and 5 kOe. (b) Temperature dependence of H_{EB} and H_C for the LSMO/SMO bilayer. Also shown are the H_C data measured for the LSMO single layer. The solid and dashed lines are the fittings to Eq. (3). The two arrows mark the Néel temperature T_N of bulk SMO and the freezing temperature T_F, respectively.

state, suggesting that the competition of the magnetic orders and the emergence of the spin glass state play important roles in the EB effect at the LSMO/SMO interface.

Furthermore, the existence of spin frustration due to the competing magnetic interactions is known to lead to an exponential temperature-dependent decay of H_{EB} and H_C, which has previously been observed in a range of diverse materials such as $Ni/Ni_{76}Mn_{24}$ bilayers,[66] $La_{1-x}Ca_xMnO_3$ ferromagnetic/antiferromagnetic superlattices,[67] and $La_{0.25}Ca_{0.75}MnO_3$ nanopaticles.[68] Indeed, the temperature dependencies of H_{EB} and H_C of LSMO/SMO bilayer in Fig. 7(b) can be fitted by the phenomenological formula

$$H_{EB}(T) = H_{EB}^0 \exp(-T/T_1)$$
$$H_C(T) = H_C^0 \exp(-T/T_2), \quad (4)$$

where H_{EB}^0 and H_C^0 are the extrapolations of H_{EB} and H_C to the absolute zero temperature; T_1 and T_2 are constants. The fitting results in Fig. 7(b) give further support to the scenario that the EB in the LSMO/SMO bilayer can be attributed to the interface spin glass state originated from the competition between the AF superexchange and the FM double-exchange interactions. However, we should note that the H_C data appear to deviate from the exponential behavior

in the high-temperature regime, suggesting the increasingly important role of thermal excitation at high temperatures.

IV. CONCLUSIONS

The magnetic properties of the LSMO/SMO bilayer appear to be quite rich, and the emergence of the spin glass state can be attributed to the competition of the AFM superexchange interaction in SMO and the FM double-exchange interaction in LSMO through the interfacial exchange coupling. This spin glass state at the FM/AFM interface further contributes to the EB effect; although the G-type AFM order in the SMO layer presents compensated spins at the interface, a uniaxial exchange anisotropy is still induced in the LSMO/SMO bilayer. Future experiments involving tools like soft x-ray and polarized neutron reflectometry are needed to explore the depth-dependent magnetic profiles in the heterostructures. In a broad perspective, the variation of spin configuration at the manganite interfaces offers opportunities to examine the outcome of competing exchange interactions and to achieve functionalities in heterostructures which are absent in individual components.

ACKNOWLEDGMENTS

We acknowledge the financial support from the Singapore National Research Foundation. S.T. gratefully acknowledges financial support from the Fund for Scientific Research Flanders (FWO) for a postdoctoral fellowship, and for funding under Project No. G.0044.13N. G.V.T. acknowledges the ERC grant COUNTATOMS. The microscope used in this study was partially financed by the Hercules Foundation of the Flemish Government.

*Present address: School of Advanced Materials Science and Engineering, Sungkyunkwan University, Suwon 440-746, Republic of Korea

†tomwu@ntu.edu.sg

[1] J. Mannhart and D. G. Schlom, Science **327**, 1607 (2010).

[2] P. Zubko, S. Gariglio, M. Gabay, P. Ghosez, and J.-M. Triscone, Annu. Rev. Cond. Mat. Phys. **2**, 141 (2011).

[3] M. Bibes, J. E. Villegas, and A. Barthélémy, Adv. Phys. **60**, 5 (2011).

[4] H. Y. Hwang, Y. Iwasa, M. Kawasaki, B. Keimer, N. Nagaosa, and Y. Tokura, Nat. Mater. **11**, 103 (2012).

[5] A. Ohtomo and H. Y. Hwang, Nature (London) **427**, 423 (2004).

[6] J. Chakhalian, J. W. Freeland, G. Srajer, J. Strempfer, G. Khaliullin, J. C. Cezar, T. Charlton, R. Dalgliesh, C. Bernhard, G. Cristiani, H. U. Habermeier, and B. Keimer, Nat. Phys. **2**, 244 (2006).

[7] J. Chakhalian, J. W. Freeland, H. U. Habermeier, G. Cristiani, G. Khaliullin, M. van Veenendaal, and B. Keimer, Science **318**, 1114 (2007).

[8] A. V. Boris, Y. Matiks, E. Benckiser, A. Frano, P. Popovich, V. Hinkov, P. Wochner, M. Castro-Colin, E. Detemple, V. K. Malik, C. Bernhard, T. Prokscha, A. Suter, Z. Salman, E. Morenzoni, G. Cristiani, H.-U. Habermeier, and B. Keimer, Science **332**, 937 (2011).

[9] M. Gibert, P. Zubko, R. Scherwitzl, J. Iniguez, and J. M. Triscone, Nat. Mater. **11**, 195 (2012).

[10] A. Bhattacharya, S. J. May, S. G. E. te Velthuis, M. Warusawithana, X. Zhai, Bin Jiang, J. M. Zuo, M. R. Fitzsimmons, S. D. Bader, and J. N. Eckstein, Phys. Rev. Lett. **100**, 257203 (2008).

[11] J. W. Seo, W. Prellier, P. Padhan, P. Boullay, J. Y. Kim, Hangil Lee, C. D. Batista, I. Martin, Elbert E. M. Chia, T. Wu, B. G. Cho, and C. Panagopoulos, Phys. Rev. Lett. **105**, 167206 (2010).

[12] N. Kida, H. Yamada, H. Sato, T. Arima, M. Kawasaki, H. Akoh, and Y. Tokura, Phys. Rev. Lett. **99**, 197404 (2007).

[13] N. M. Nemes, M. García-Hernández, S. G. E. te Velthuis, A. Hoffmann, C. Visani, J. Garcia-Barriocanal, V. Peña, D. Arias, Z. Sefrioui, C. Leon, and J. Santamaría, Phys. Rev. B **78**, 094515 (2008).

[14] L. You, C. L. Lu, P. Yang, G. C. Han, T. Wu, U. Luders, W. Prellier, K. Yao, L. Chen, and J. L. Wang, Adv. Mater. **22**, 4964 (2010).

[15] X. Ke, M. S. Rzchowski, L. J. Belenky, and C. B. Eom, Appl. Phys. Lett. **84**, 5458 (2004).

[16] M. Ziese, I. Vrejoiu, E. Pippel, P. Esquinazi, D. Hesse, C. Etz, J. Henk, A. Ernst, I. V. Maznichenko, W. Hergert, and I. Mertig, Phys. Rev. Lett. **104**, 167203 (2010).

[17] V. Thakare, G. Z. Xing, H. Y. Peng, A. Rana, O. Game, P. A. Kumar, A. Banpurkar, Y. Kolekar, K. Ghosh, T. Wu, D. D. Sarma, and S. B. Ogale, Appl. Phys. Lett. **100**, 172412 (2012).

[18] K. Ueda, H. Tabata, and T. Kawai, Science **280**, 1064 (1998).

[19] T. Koida, M. Lippmaa, T. Fukumura, K. Itaka, Y. Matsumoto, M. Kawasaki, and H. Koinuma, Phys. Rev. B **66**, 144418 (2002).

[20] Ş. Smadici, P. Abbamonte, A. Bhattacharya, X. Zhai, B. Jiang, A. Rusydi, J. N. Eckstein, S. D. Bader, and J. M. Zuo, Phys. Rev. Lett. **99**, 196404 (2007).

[21] H. Yamada, P. H. Xiang, and A. Sawa, Phys. Rev. B **81**, 014410 (2010).

[22] J. W. Seo, B. T. Phan, J. Stahn, J. Lee, and C. Panagopoulos, Phys. Rev. B **82**, 140405 (2010).

[23] W. H. Meiklejohn, J. Appl. Phys. **33**, 1328 (1962).

[24] A. P. Malozemoff, Phys. Rev. B **37**, 7673 (1988).

[25] A. P. Malozemoff, Phys. Rev. B **35**, 3679 (1987).

[26] N. C. Koon, Phys. Rev. Lett. **78**, 4865 (1997).

[27] T. C. Schulthess and W. H. Butler, Phys. Rev. Lett. **81**, 4516 (1998).

[28] M. Kiwi, J. Mejia-Lopez, R. D. Portugal, and R. Ramirez, Appl. Phys. Lett. **75**, 3995 (1999).

[29] M. Kiwi, J. Magn. Magn. Mater. **234**, 584 (2001).

[30] U. Nowak, K. D. Usadel, J. Keller, P. Miltényi, B. Beschoten, and G. Güntherodt, Phys. Rev. B **66**, 014430 (2002).

[31] S. Dong, K. Yamauchi, S. Yunoki, R. Yu, S. H. Liang, A. Moreo, J. M. Liu, S. Picozzi, and E. Dagotto, Phys. Rev. Lett. **103**, 127201 (2009).

[32] H. Bea, M. Bibes, S. Cherifi, F. Nolting, B. Warot-Fonrose, S. Fusil, G. Herranz, C. Deranlot, E. Jacquet, K. Bouzehouane, and A. Barthelemy, Appl. Phys. Lett. **89**, 242114 (2006).

[33] J. Dho, X. Qi, H. Kim, J. L. MacManus-Driscoll, and M. G. Blamire, Adv. Mater. **18**, 1445 (2006).
[34] Y. H. Chu, L. W. Martin, M. B. Holcomb, M. Gajek, S. J. Han, Q. He, N. Balke, C. H. Yang, D. Lee, W. Hu, Q. Zhan, P. L. Yang, A. Fraile-Rodriguez, A. Scholl, S. X. Wang, and R. Ramesh, Nat. Mater. **7**, 478 (2008).
[35] L. W. Martin, Y. H. Chu, M. B. Holcomb, M. Huijben, P. Yu, S. J. Han, D. Lee, S. X. Wang, and R. Ramesh, Nano Lett. **8**, 2050 (2008).
[36] H. Béa, M. Bibes, F. Ott, B. Dupé, X. H. Zhu, S. Petit, S. Fusil, C. Deranlot, K. Bouzehouane, and A. Barthélémy, Phys. Rev. Lett. **100**, 017204 (2008).
[37] A. P. Ramirez, J. Phys.: Condens. Matter **9**, 8171 (1997).
[38] J. M. D. Coey, M. Viret, and S. von Molnár, Adv. Phys. **48**, 167 (1999).
[39] Y. Tokura, Rep. Prog. Phys. **69**, 797 (2006).
[40] I. Panagiotopoulos, C. Christides, N. Moutis, M. Pissas, and D. Niarchos, J. Appl. Phys. **85**, 4913 (1999).
[41] I. Panagiotopoulos, C. Christides, M. Pissas, and D. Niarchos, Phys. Rev. B **60**, 485 (1999).
[42] I. Panagiotopoulos, C. Christides, D. Niarchos, and M. Pissas, J. Appl. Phys. **87**, 3926 (2000).
[43] O. Moran, M. E. Gomez, J. G. Ramirez, T. Schwarz, D. Fuchs, R. Hott, and R. Schneider, J. Appl. Phys. **97**, 10K116 (2005).
[44] I. N. Krivorotov, K. R. Nikolaev, A. Yu Dobin, A. L. Kobrinskii, R. Wentzcovitch, A. M. Goldman, and E. D. Dahlberg, J. Appl. Phys. **89**, 6964 (2001).
[45] A. L. Kobrinskii, A. M. Goldman, M. Varela, and S. J. Pennycook, Phys. Rev. B **79**, 094405 (2009).
[46] M. T. Fernández-Díaz, J. L. Martínez, J. M. Alonso, and E. Herrero, Phys. Rev. B **59**, 1277 (1999).
[47] W. S. Choi, Z. Marton, S. Y. Jang, S. J. Moon, B. C. Jeon, J. H. Shin, S. S. A. Seo, T. W. Noh, K. Myung-Whun, H. N. Lee, and Y. S. Lee, J. Phys. D: Appl. Phys. **42**, 165401 (2009).
[48] R. Mahendiran, S. K. Tiwary, A. K. Raychaudhuri, T. V. Ramakrishnan, R. Mahesh, N. Rangavittal, and C. N. R. Rao, Phys. Rev. B **53**, 3348 (1996).
[49] O. Chmaissem, B. Dabrowski, S. Kolesnik, J. Mais, J. D. Jorgensen, and S. Short, Phys. Rev. B **67**, 094431 (2003).
[50] M. Gruyters, Phys. Rev. Lett. **95**, 077204 (2005).
[51] J. Alonso, M. L. Fdez-Gubieda, J. M. Barandiarán, A. Svalov, L. Fernández Barquín, D. Alba Venero, and I. Orue, Phys. Rev. B **82**, 054406 (2010).
[52] S. Mukherjee, R. Ranganathan, P. S. Anilkumar, and P. A. Joy, Phys. Rev. B **54**, 9267 (1996).
[53] X. H. Huang, J. F. Ding, Z. L. Jiang, Y. W. Yin, Q. X. Yu, and X. G. Li, J. Appl. Phys. **106**, 083904 (2009).
[54] X. G. Li, X. J. Fan, G. Ji, W. B. Wu, K. H. Wong, C. L. Choy, and H. C. Ku, J. Appl. Phys. **85**, 1663 (1999).
[55] B. Xavier and L. Amílcar, J. Phys. D: Appl. Phys. **35**, R15 (2002).
[56] M. B. Salamon and M. Jaime, Rev. Mod. Phys. **73**, 583 (2001).
[57] K. Binder and A. P. Young, Rev. Mod. Phys. **58**, 801 (1986).
[58] S. D. Tiwari and K. P. Rajeev, Phys. Rev. B **72**, 104433 (2005).
[59] D. N. H. Nam, K. Jonason, P. Nordblad, N. V. Khiem, and N. X. Phuc, Phys. Rev. B **59**, 4189 (1999).
[60] R. V. Chamberlin, J. Appl. Phys. **57**, 3377 (1985).
[61] M. K. Singh, W. Prellier, M. P. Singh, Ram S. Katiyar, and J. F. Scott, Phys. Rev. B **77**, 144403 (2008).
[62] H. B. Zhao, K. J. Smith, Y. Fan, G. Lüpke, A. Bhattacharya, S. D. Bader, M. Warusawithana, X. Zhai, and J. N. Eckstein, Phys. Rev. Lett. **100**, 117208 (2008).
[63] H. Tanaka and T. Kawai, J. Appl. Phys. **88**, 1559 (2000).
[64] S. J. May, P. J. Ryan, J. L. Robertson, J. W. Kim, T. S. Santos, E. Karapetrova, J. L. Zarestky, X. Zhai, S. G. E. te Velthuis, J. N. Eckstein, S. D. Bader, and A. Bhattacharya, Nat. Mater. **8**, 892 (2009).
[65] M. D. Stiles and R. D. McMichael, Phys. Rev. B **60**, 12950 (1999).
[66] B. Aktas, Y. Öner, and H. Z. Durusoy, J. Magn. Magn. Mater. **119**, 339 (1993).
[67] N. Moutis, C. Christides, I. Panagiotopoulos, and D. Niarchos, Phys. Rev. B **64**, 094429 (2001).
[68] X. H. Huang, J. F. Ding, G. Q. Zhang, Y. Hou, Y. P. Yao, and X. G. Li, Phys. Rev. B **78**, 224408 (2008).